Mechanical and Covalent Tailoring of Copper Catenanes for Selective Aqueous Nitrate-to-Ammonia Electrocatalysis

Yulin Deng[1,‡], Xiaoyong Mo[1,‡], Samuel Kin-Man Lai[1], Shu-Chih Haw[2], Ho Yu Au-Yeung[1,3,*], Edmund C. M. Tse[1,*]

[1] HKU-CAS Joint Laboratory on New Materials & Department of Chemistry, The University of Hong Kong, Pokfulam Road, Hong Kong SAR, P. R. China

[2] National Synchrotron Radiation Research Center, 101 Hsin-Ann Road, Hsinchu 30076, Taiwan

[3] State Key Laboratory of Synthetic Chemistry, The University of Hong Kong, Pokfulam Road, Hong Kong SAR, P. R. China

[‡] Equal contribution

* Corresponding authors: HYAY: hoyuay@hku.hk; ECMT: ecmtse@hku.hk

Abstract

Electrocatalytic nitrate reduction reaction (NO_3RR) for selective generation of ammonia (NH_3) enables the removal of deleterious nitrate pollutants while simultaneously upcycling them into value-added fertilizer. The development of nonprecious metal-derived catalysts such as those featuring copper (Cu) as earth-abundant alternatives for the state-of-the-art precious metal catalysts is of urgent need yet suffering from the activity-selectivity-durability trilemma. Rational design of molecular Cu complexes with well-defined coordination structures permitting systematic structure-activity relationship (SAR) investigations is key to addressing the challenge. Here, a series of molecular Cu(I) complexes with [2]catenane ligands are developed as NO_3RR electrocatalysts for the first time. By engineering of multiple cationic ammoniums on the catenane backbone, acceptance of the anionic nitrate substrate as well as the release of the cationic ammonium product are promoted, thereby facilitating a higher Faradaic efficiency and product selectivity towards ammonia via an $8e^-$ pathway. Of note, the mutual Coulombic repulsion between the multiply charged ligands is overcome by the mechanical interlocking such that the catalyst integrity can be maintained under practical conditions. This report highlights the promise of employing mechanically interlocked ligands as a platform for customizing metal complexes as catalysts for redox processes involving multiple proton-coupled electron transfer steps.

Introduction

Closing the artificial nitrogen cycle is key to a sustainable society. The efficient removal of excessive nitrate (NO_3^-) and other nitrogen-containing pollutants from effluents, as well as their simultaneous upcycling into value-added fertilizer (e.g. ammonia NH_3) is one central technology for achieving this goal.[1-3] In contrast to some common strategies for nitrate removal such as membrane technology, reverse osmosis, electrodialysis, and biological denitrification,[4-10] electrocatalytic nitrate reduction is an environmentally friendly alternative that can remove and convert nitrate into ammonia via consecutive proton-coupled electron transfer (PCET) ($NO_3^- + 9H^+ + 8e^- \rightarrow NH_3 + 3H_2$) under ambient condition without additional oxygenation processes.[11-15] Although the low-temperature nitrate-to-ammonia conversion method is promising, developing catalysts with high activity and selectivity towards ammonia remains challenging due to (1) the sluggish reduction kinetics, (2) multiple parallel pathways generating a mixture of products, and (3) the competitive hydrogen evolution reaction (HER) at the cathode.[16-20]

Currently studied electrocatalysts for nitrate reduction reaction (NO_3RR) are mainly clusters, nanoalloys or nanoparticles derived from precious metals such as Pt, Pd, Ru, and Rh.[21-24] While efficient and selective reduction of nitrate with Faradaic efficiency (FE) as high as 100% has been demonstrated by some of these precious metal catalysts, the high cost of the precious metals has prohibited their practical application. In this regard, non-precious metal (NPM) catalysts have been investigated as cost effective and scalable alternatives.[25] Copper (Cu) is particularly attractive due to its low cost, earth abundance, strong nitrate adsorption capability, and fast electron transfer kinetics. Previous studies involving Cu-based nanoalloys for NO_3RR were fabricated by surface engineering that tunes the surface nitrate coverage to achieve simultaneous enhancement in activity and selectivity.[26-27] Despite decades of efforts in developing earth-abundant nanomaterials for electrocatalytic NO_3RR, the activity-selectivity-durability trilemma is hard to be overcome due to limitations in tuning precisely the active site structure at an atomic level.[28-29]

With their well-defined coordination structures, molecular transition metal complexes that are amenable for systematic structure-activity relationship (SAR) investigations will allow a more precise control and tuning of the catalytic performance through rational ligand design. For example, inspired by the active site structure of copper nitrite reductases, Cu(II)-bis(pyridyl)amine complexes have been utilized for the selective reduction of nitrite (NO_2^-) into NO, and the relationship between the primary coordination structure and

catalytic performance has been revealed by SAR studies with various ligand analogues.[30] Yet, different than the deeply buried metal active sites in metalloenzymes,[31-34] molecular copper complexes are usually labile, and the rapid ligand exchange involving Cu^{+} or Cu^{2+} ions could generate multiple copper species with ill-defined coordination environment during the catalysis,[35-36] which not only complicate the SAR and mechanistic studies of the NO_3RR, but also the activity, selectivity and durability of the catalyst will be compromised.

Mechanical interlocking of coordination ligand is one effective way to circumvent issues due to the rapid ligand exchange of the labile copper.[37-40] When mechanically interlocked molecules (MIMs), such as catenanes are employed as ligand, complete ligand dissociation is prohibited and hence ligand scrambling is efficiently minimized.[41-46] On one hand, the kinetic stability from the catenane ligand will help maintaining a well-defined coordination environment and sustaining the catalyst activity and selectivity despite the different oxidation state, coordination number and geometry of the copper at different stages of the catalysis.[46-47] On the other hand, the dynamic coordination would allow substrates to access the metal active site, and the restrictions imposed by the interlocked ligands could also promote turn-over, facilitate H^{+}/e^{-} transfer, orient the substrate and steer the catalysis towards specific pathways to improve activity and selectivity.[48-49]

Herein, we report the development of catenane-supported Cu(I) molecular catalysts for electrocatalytic NO_3RR. Specifically, it is hypothesized that by engineering multiple cationic charges on the catenane backbone, acceptance of the negatively charged NO_3^{-} substrate, as well as release of the positively charged product NH_4^{+} will be facilitated to promote catalytic activity and product selectivity.[50] In addition, size effect of the catenane ligands, which has been shown to influence catalytic activity and selectivity of Cu(I) catenane complexes, was also investigated.[47-48, 51]

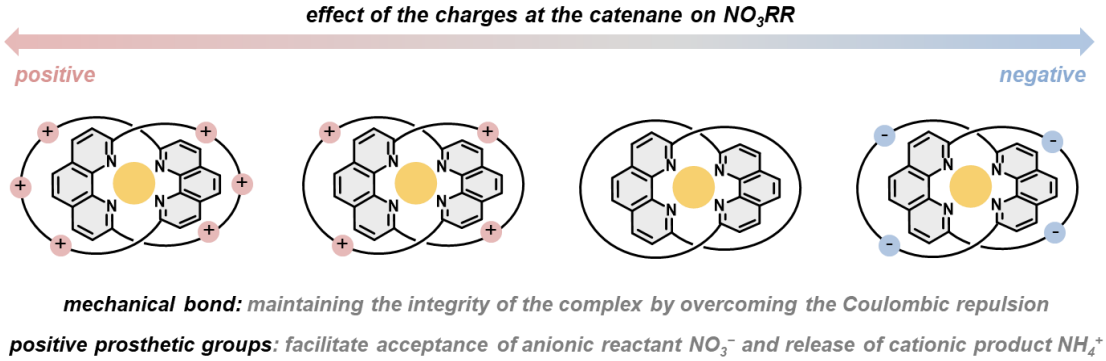

Figure 1. Effect of prosthetic groups of the Cu(I) catenane complexes on electrocatalytic nitrate reduction.

Results and Discussion

A series of Cu(I) catenane complexes, differed by the number of cationic ammonium groups, as well as the size of the interlocked macrocycles, were prepared and studied as electrocatalysts for NO_3RR (Figures 2, 6a). Of note, due to the mutual Coulombic repulsion between the cationic ammoniums, integrity of these labile Cu(I) complexes is only maintained in the presence of the mechanical bond, or otherwise equilibrating mixtures of Cu(I) species of various ligand stoichiometry, nuclearity, and number of coordinated solvents will be resulted, thus highlighting the unique role of mechanical interlocking in obtaining these molecular catalysts in kinetically stable forms.[51] Synthesis of these Cu(I) catenane complexes is straightforward with only few steps (see ESI for details).[52]

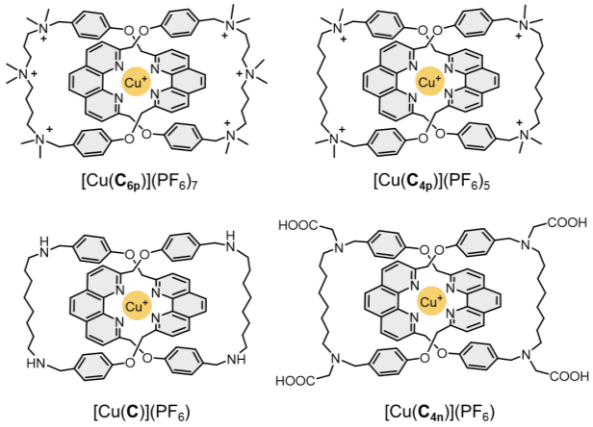

Figure 2. Structures of the Cu(I) catenane electrocatalysts. [Cu(**C**$_{6p}$)](PF$_6$)$_7$ and [Cu(**C**$_{4p}$)](PF$_6$)$_5$ are supported by a [2]catenane ligand that incorporates six and four ammonium units, respectively. [Cu(**C**$_{4n}$)](PF$_6$) contains four carboxylic acids that exchange with carboxylates under experimental conditions.

Effects of the cationic ammonium groups on the Cu coordination structure are first studied by ^{1}H NMR (Figure 3). Due to the electrostatic repulsion between the ammoniums on the catenane backbone, the interlocked macrocycles in [Cu(**C**$_{6p}$)](PF$_6$)$_7$ and [Cu(**C**$_{4p}$)](PF$_6$)$_5$ are likely adopting a more "open" conformation when compared to [Cu(**C**)](PF$_6$). For example, the H_{Ar} resonances of the two former complexes were found to be more downfield by 0.28–0.37 ppm than that of the latter, which is consistent to a looser, less efficient π-stacking interactions of the phenyl units with the phenanthroline. On the other hand, [Cu(**C**$_{6p}$)](PF$_6$)$_7$ is mechanically chiral because of the directionality in the macrocycles and exists as a racemic mixture, which is evidenced by the diastereotopic splitting of OCH_2 and $ArCH_2N$ resonances.

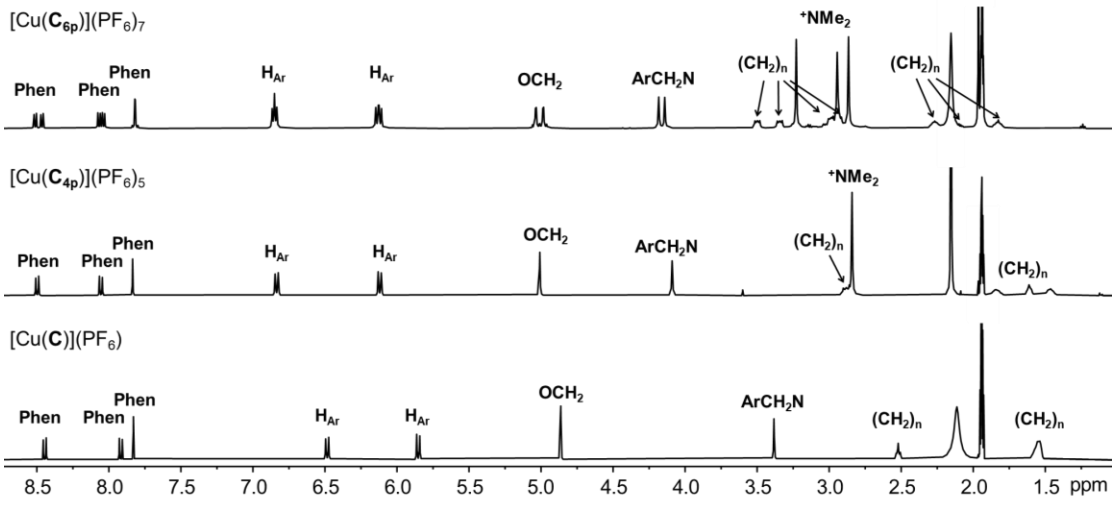

Figure 3. ^{1}H NMR spectra (500 MHz, CD_3CN, 298 K) of [Cu(**C$_{6p}$**)](PF$_6$)$_7$, [Cu(**C$_{4p}$**)](PF$_6$)$_5$, and [Cu(**C**)](PF$_6$).

Effects of the cationic ammonium groups on the redox properties of the Cu(I) catenane complexes are next explored by X-ray techniques and voltammetry. Figures 4a and S13 show the X-ray photoelectron spectra (XPS) of [Cu(**C$_{6p}$**)](PF$_6$)$_7$, [Cu(**C$_{4p}$**)](PF$_6$)$_5$, [Cu(**C**)](PF$_6$) and [Cu(**C$_{4n}$**)](PF$_6$). The oxidation state of Cu is determined to be 1+ (BE = c.a. 932 eV) regardless of the number of ammonium groups in the catenane. Figure 4b shows the Cu L3-edge X-ray absorption spectra (XAS) collected in total electron yield (TEY) mode of pristine [Cu(**C$_{6p}$**)](PF$_6$)$_7$ and its carbon-supported version ([Cu(**C$_{6p}$**)](PF$_6$)$_7$/Vulcan). The Cu centre in pristine [Cu(**C$_{6p}$**)](PF$_6$)$_7$ and [Cu(**C$_{6p}$**)](PF$_6$)$_7$/Vulcan remains as Cu(I), indicating that the carbon substrate does not affect the oxidation state of the Cu(I) catenane complexes physically adsorbed on mesoporous Vulcan. The electrochemical behaviors of [Cu(**C$_{4n}$**)](PF$_6$), [Cu(**C**)](PF$_6$), and [Cu(**C$_{6p}$**)](PF$_6$)$_7$ are further investigated using cyclic voltammetry (CV). Of note, p*K*a values of the four carboxyl groups in [Cu(**C$_{4n}$**)](PF$_6$) are estimated to be 1.6, 2.8, 4.4, and 6.1, suggesting that ca. 90% of the catenane complexes exist in the form with four anionic COO^- pendants under the experimental conditions (pH = 7). Figure S14a shows the CV curves of [Cu(**C$_{4n}$**)](PF$_6$) (green), [Cu(**C**)](PF$_6$) (pink), and [Cu(**C$_{6p}$**)](PF$_6$)$_7$ (blue) supported on Vulcan carbon in N_2-saturated pH 7 buffer. [Cu(**C$_{6p}$**)](PF$_6$)$_7$ displays positive shifts in both the oxidation (E_{pa}) and reduction (E_{pc}) potentials of the $Cu^{II/I}$ redox couple to 0.92 V and 0.62 V, respectively, from 0.89 V and 0.58 V of [Cu(**C**)](PF$_6$) and [Cu(**C$_{4n}$**)](PF$_6$) (Figure S14b), suggesting that the cationic [2]catenane ligand can indeed modulate the redox properties of the coordinated Cu(I), which is consistent with previous findings.[51]

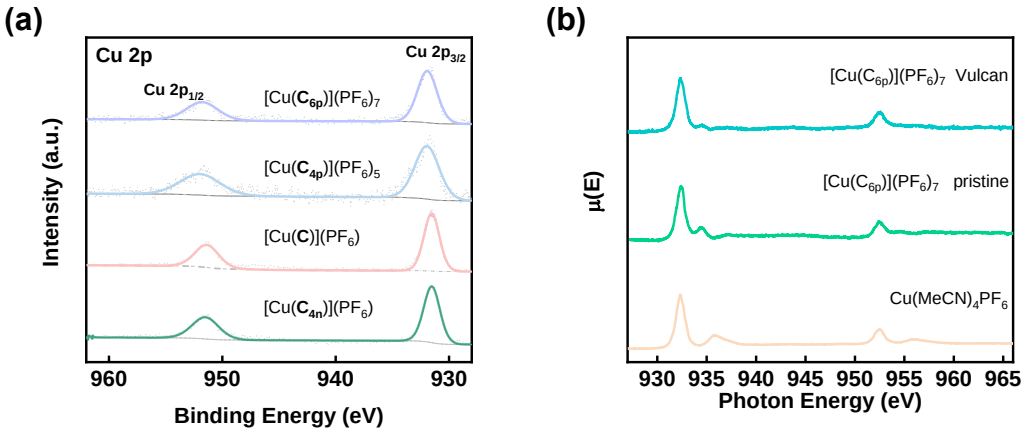

Figure 4. X-ray spectroscopy techniques for Cu centre characterization. (a) High-resolution XPS of X-ray photoelectron spectra (XPS) Cu 2p in of [Cu(**C6p**)](PF6)7(purple), [Cu(**C4p**)](PF6)5 (blue), [Cu(**C**)](PF6) (pink), and [Cu(**C4n**)](PF6) (green). (b) Cu L3-edge X-ray absorption spectra (XAS) of Cu(MeCN)4(PF6) reference (bisque) and [Cu(**C6p**)](PF6)7 pristine (caribbean green) and [Cu(**C6p**)](PF6)7 supported on Vulcan (turquoise). XAS were collected in total electron yield (TEY) mode.

Effect of Ammonium Groups on the Electrocatalytic Nitrate Reduction Activity and Product Selectivity of Mechanically Interlocked Cu Complexes

The electrocatalytic nitrate reduction performance of [Cu(**C4p**)](PF6)5, [Cu(**C**)](PF6), and [Cu(**C4n**)](PF6) are evaluated using linear sweep voltammetry (LSV) to study the effect of prosthetic groups on the [2]catenane backbone on the catalytic performances, and their catalytic activities are normalized on a per mass of Cu basis. In the absence of nitrate, Figure 5a shows that the onset potentials of hydrogen evolution reaction (HER) for all three Cu(I) catenane complexes are observed at -0.53 V vs. RHE (Figure 5a, dash line). Upon the addition of nitrate, all as-prepared Cu(I) complexes display a positive shift in onset potentials to -0.38 V vs. RHE with a concomitant increase in mass activities, indicating that nitrate reduction likely overtakes HER as the dominant and more facile process when nitrate is present in the solution. [Cu(**C4p**)](PF6)5 exhibits excellent nitrate reduction activity (Figure 5a, blue solid line) as compared with [Cu(**C**)](PF6) (Figure 5a, red solid line) and [Cu(**C4n**)](PF6)5 (Figure 5a, olive solid line). These results likely suggests that the charged appendages on the catenanes can impact the electrocatalytic nitrate reduction activity of Cu(I) catenane complexes. To further examine the effect of the number of ammonium groups on the electrocatalytic performance, the nitrate

reduction mass activity of [Cu(**C$_{6p}$**)](PF$_6$)$_7$ is compared with that of [Cu(**C$_{4p}$**)](PF$_6$)$_5$ (Figure 5a and b). The normalized LSV results show that the onset potential of [Cu(**C$_{6p}$**)](PF$_6$)$_7$ shifts to the positive direction by ~50 mV relative to that of [Cu(**C$_{4p}$**)](PF$_6$)$_5$ at the same mass activity (0.5 A·mg^{-1}), corroborating that [Cu(**C$_{6p}$**)](PF$_6$)$_7$ is the most efficient for electrocatalytic nitrate reduction among the Cu(I) catenanes tested.

To achieve a more comprehensive understanding of the relationship between the charged substituents on the catenane ligand and the nitrate reduction performance of the overall complex, we next analyze the products generated from nitrate reduction catalyzed by these three Cu(I) catenane complexes after subjecting them to a constant potential treatment at -0.8 V vs. RHE. Three main nitrate reduction products, namely nitrite (NO_2^-), hydroxylamine (NH_2OH), and ammonia (NH_3), are detected and quantified. The quantity of nitrite is measured by ion chromatography (IC). UV-Vis spectroscopy is utilized to quantify the amount of hydroxylamine generated after treating the crude product with $K_3Fe(CN)_6$ under a strong alkaline condition. Ammonia is also quantified using UV-Vis spectroscopy via a colorimetric assay based on indophenol blue (Figure S16). Upon holding at -0.8 V vs. RHE for 30 min, the Faradaic efficiencies (FE) for NO_2^- (54%) and NH_3 (52%) obtained for [Cu(**C$_{4n}$**)](PF$_6$)/Vulcan are similar. In contrast, [Cu(**C**)](PF$_6$)/Vulcan, [Cu(**C$_{4p}$**)](PF$_6$)$_5$/Vulcan and [Cu(**C$_{6p}$**)](PF$_6$)$_7$/Vulcan exhibit a much lower FE for nitrite (ca. 14%, 14%, and 5%, respectively) while simultaneously yielding an elevated FE for ammonia (ca. 65%, 74%, and 86%, respectively) (Figure 5c). In addition, the NO_3^- conversion rates catalyzed by [Cu(**C**)](PF$_6$)/Vulcan, [Cu(**C$_{4p}$**)](PF$_6$)$_5$/Vulcan, and [Cu(**C$_{6p}$**)](PF$_6$)$_7$/Vulcan are determined to be 1.08%, 1.13% and 8.3% respectively (Figure S17a). The selectivity towards ammonia of [Cu(**C$_{6p}$**)](PF$_6$)$_7$ (76%) is found to be higher than that of [Cu(**C**)](PF$_6$) (52%), [Cu(**C$_{4p}$**)](PF$_6$)$_5$ (56%), and [Cu(**C$_{4n}$**)](PF$_6$) (19%) (Figure 5f). Only a small amount of NH_2OH can be detected for all these complexes. Although [Cu(**C$_{6p}$**)](PF$_6$)$_7$ displays the highest FE and selectivity toward NH_3, the turnover frequency (TOF) and yield rate of [Cu(**C$_{6p}$**)](PF$_6$)$_7$ are similar to those of [Cu(**C**)](PF$_6$) (Figures 5d and e), indicating that the Cu sites in [Cu(**C**)](PF$_6$) are more active, but less selective, than those in [Cu(**C$_{6p}$**)](PF$_6$)$_7$. In the case of [Cu(**C$_{4p}$**)](PF$_6$)$_5$ and [Cu(**C$_{6p}$**)](PF$_6$)$_7$, the ammonium groups on the methylene chain of the catenane ligand likely assist the acceptance of NO_3^- by the Cu(I) site as well as promote electron and proton transfer during the product formation step. In contrast, the negatively charged carboxylate units in

[Cu(**C$_{4n}$**)](PF$_6$), an anionic complex in the resting state, lead to an unfavorable microenvironment for NO_3^- absorption, thereby inhibiting the subsequent reduction steps of NO_3^- and limiting the overall NH_3 selectivity.

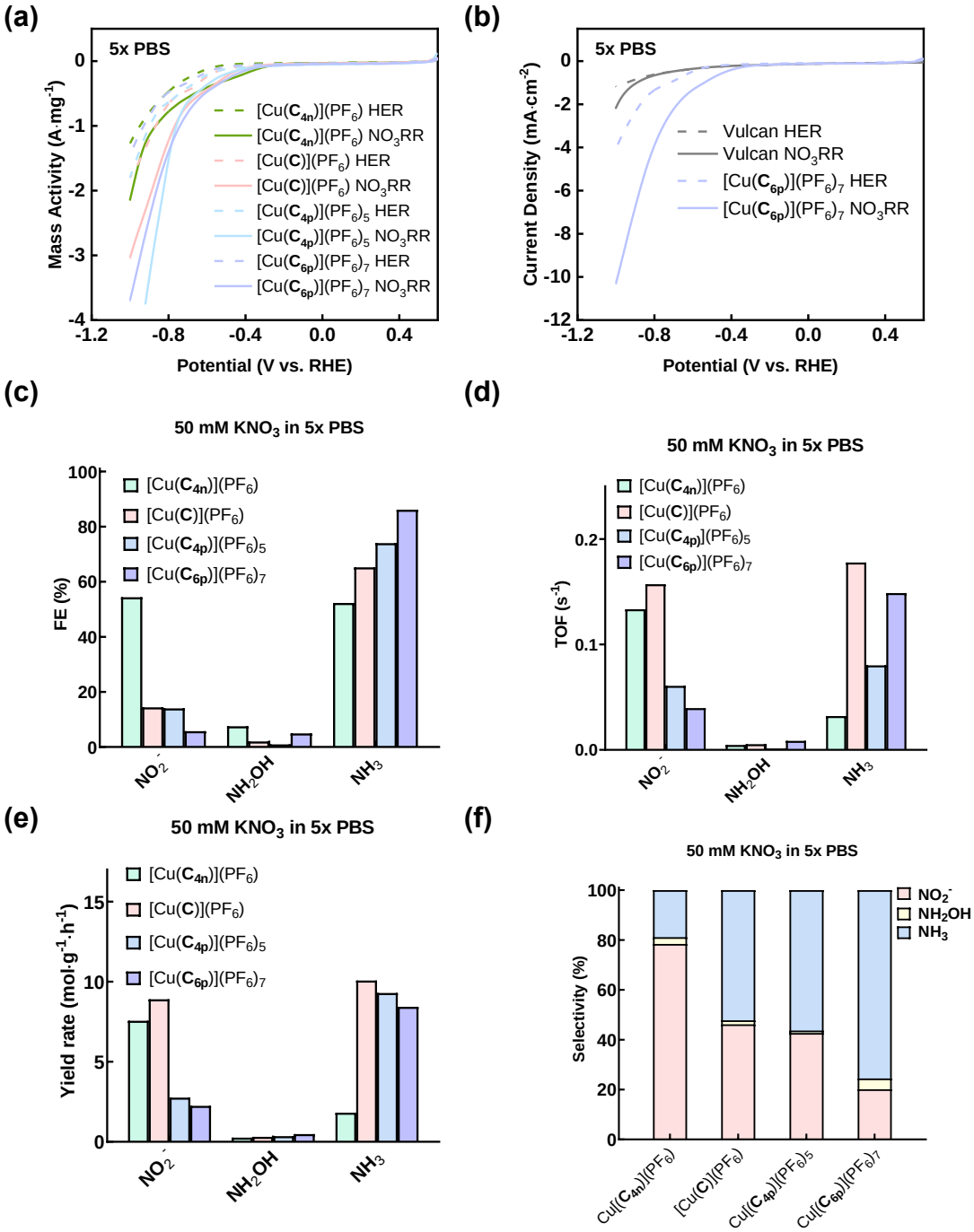

Figure 5. Impact of charged substituents on the electrocatalytic performance of the Cu(I) catenanes. (a) Mass activity of NO_3RR (solid line) and HER (dashed line) in pH 7 Ar-saturated 5x PBS catalyzed by [Cu(**C4n**)](PF_6) (green), [Cu(**C**)](PF_6) (pink), [Cu(**C4p**)]$(PF_6)_5$ (blue), and [Cu(**C6p**)]$(PF_6)_7$ (purple). (b) Comparison of HER and NO_3RR performance catalyzed [Cu(**C6p**)]$(PF_6)_7$ and Vulcan only. (c) Faradaic efficiency (FE), (d) turnover frequency (TOF), and (e) yield rate of NH_3, NH_2OH, and NO_2^- obtained by [Cu(**C4n**)](PF_6) (green), [Cu(**C**)](PF_6) (pink), [Cu(**C4p**)]$(PF_6)_5$ (blue), and [Cu(**C6p**)]$(PF_6)_7$ (purple) at -0.8 V vs. RHE. (f) Product selectivity of [Cu(**C4n**)](PF_6), [Cu(**C**)](PF_6), [Cu(**C4p**)]$(PF_6)_5$, and [Cu(**C6p**)]$(PF_6)_7$ at -0.8 V vs. RHE.

Kinetic isotope effect (KIE) studies are subsequently conducted to gain insights into the role of protons during nitrate reduction. Upon deuteration, the onset potentials of the tested Cu(I) complexes display minimal negative shifts by only 0.02 V (Figure S18a), suggesting minimal equilibrium isotope effect (EIE). The selectivity of [Cu(**C$_{4n}$**)](PF$_6$) does not show obvious differences upon deuteration with NO_2^- still being the dominant product (Figure S18f), suggesting that the carboxylate appendages do not impart product selectivity on the Cu centre upon switching to pD 7. In contrast, NO_2^- emerges as the major product for [Cu(**C**)](PF$_6$)/Vulcan (72%) and [Cu(**C$_{6p}$**)](PF$_6$)$_7$/Vulcan (75%) in deutero solutions (Figure S18f). Altering the product selectivity from NQ_3 (Q = H or D) in proteo solutions to nitrite in deutero solutions indicate that slow proton/deuteron transfer impedes HER/DER as well as reduction steps in NO_3RR, resulting in partial conversion of NO_3^- into NO_2^- via a $2e^-/2H^+$ pathway. Upon switching from deutero to proteo solutions, [Cu(**C**)](PF$_6$)/Vulcan displays a ~15% increase in FE of NQ_3 while [Cu(**C$_{6p}$**)](PF$_6$)$_7$/Vulcan exhibits a ~40% increase in FE of NQ_3. The more drastic increase in NQ_3 selectivity for [Cu(**C$_{6p}$**)](PF$_6$)$_7$/Vulcan corroborates that the ammonium groups on the methylene chain of the ligand on [Cu(**C$_{6p}$**)](PF$_6$)$_7$ facilitate the downstream $8e^-/9H^+$ steps to form NH_3 after initial NO_3^- acceptance by the Cu centre.

The cathodic current density obtained on [Cu(**C$_{4n}$**)](PF$_6$)/Vulcan is much higher than those on [Cu(**C**)](PF$_6$)/Vulcan and [Cu(**C$_{6p}$**)](PF$_6$)$_7$/Vulcan at -0.8 V vs. RHE (Figures S18b). This trend observed in deutero solution is opposite to the trend observed in the proteo cases (Figure S19) and can also be rationalized by the selectivity change. Since [Cu(**C$_{4n}$**)](PF$_6$)/Vulcan prefers the $2e^-/2H^+$ pathway to generate NO_2^- from NO_3^- regardless of whether the reaction is conducted in pH 7 or pD 7, the amount of current passed remains similar in both cases. For [Cu(**C**)](PF$_6$)/Vulcan and [Cu(**C$_{6p}$**)](PF$_6$)$_7$/Vulcan, since proton transfer is faster than deuteron transfer, they both change from a $2e^-/2H^+$ pathway to a $8e^-/9H^+$ pathway. Upon switching the product selectivity from nitrite in pD7 to ammonia in pH 7, a corresponding increase in cathodic currents is thus observed. Moreover, the FE, TOF, and yield rate of NQ_3 on [Cu(**C**)](PF$_6$)/Vulcan and [Cu(**C$_{6p}$**)](PF$_6$)$_7$/Vulcan decrease while those of nitrite increase in deutero solutions as compared with proteo solution (Figures S18c, d and e). Taken together, these observations suggest that the charged appendages on the catenanes on [Cu(**C$_{6p}$**)](PF$_6$)$_7$ and [Cu(**C$_{4n}$**)](PF$_6$) influence the Cu(I) site regarding NO_3^- binding and proton delivery, thereby modulating the nitrate reduction activity and product selectivity.

Effect of the Catenane Ring Size on Electrocatalytic Nitrate Reduction Activity and Product Selectivity

Next, [Cu(**C**)](PF_6)/Vulcan featuring a neutral ligand is chosen to be further explored because [Cu(**C**)](PF_6)/Vulcan displays the highest TOF and yield rate for nitrate-to-ammonia reduction. In particular, because the geometry changes, as well as the associated kinetics and thermodynamics, between tetrahedral and square planar forms of the Cu(I/II) during the PCET steps would be affected by the co-conformational flexibility of the mechanical interlocking, length of the methylene linkers in the [2]catenane ligands are varied to investigate the ring size effect on the overall electrocatalytic performance of the resulting Cu(I) complexes. Figure 6 shows the nitrate reduction FE, TOF, yield rate, and product selectivity when using Vulcan-supported [Cu(**C**)](PF_6), [Cu(**C′**)](PF_6), and [Cu(**C″**)](PF_6) as the electrocatalysts featuring respectively C_8, C_{10} and C_{12} linkers in the catenane backbone. Although [Cu(**C**)](PF_6) and [Cu(**C′**)](PF_6) display similar nitrate reduction onset potentials (-0.38 V vs. RHE), the cathodic current density of [Cu(**C′**)](PF_6) is higher than that of [Cu(**C**)](PF_6). [Cu(**C″**)](PF_6) is found to be less active for nitrate reduction with an additional 200 mV overpotential relative to the [Cu(**C**)](PF_6) and [Cu(**C′**)](PF_6) cases (Figure 6b), suggesting that the ring size and (co)conformational dynamics of the catenanes can alter their electrocatalytic attributes. Three main products including NH_3, NH_2OH, and NO_2^- are detected in the nitrate reduction process catalyzed by Vulcan-supported [Cu(**C**)](PF_6), [Cu(**C′**)](PF_6), and [Cu(**C″**)](PF_6). Upon lengthening the C_8 aliphatic linker in **C** to the C_{12} linker in **C″**, NH_3 remains as the major product for all three Cu(I)catenane catalysts. Intriguingly, [Cu(**C′**)](PF_6) exhibits the highest FE (95%), TOF (0.30 s^{-1}), yield rate (17 mol g^{-1} h^{-1}), and NH_3 selectivity (70%). Furthermore, [Cu(**C′**)](PF_6) also displays the highest NO_3^- conversion rate of 13.1% (Figure S20b). The observed trend in the nitrate reduction activity and product selectivity could be rationalized by the energetics of the [2]catenane ligands undergoing optimal (co)conformational changes for accepting the NO_3^- substrate and mediating reduction of intermediates and downstream electron transfer steps.

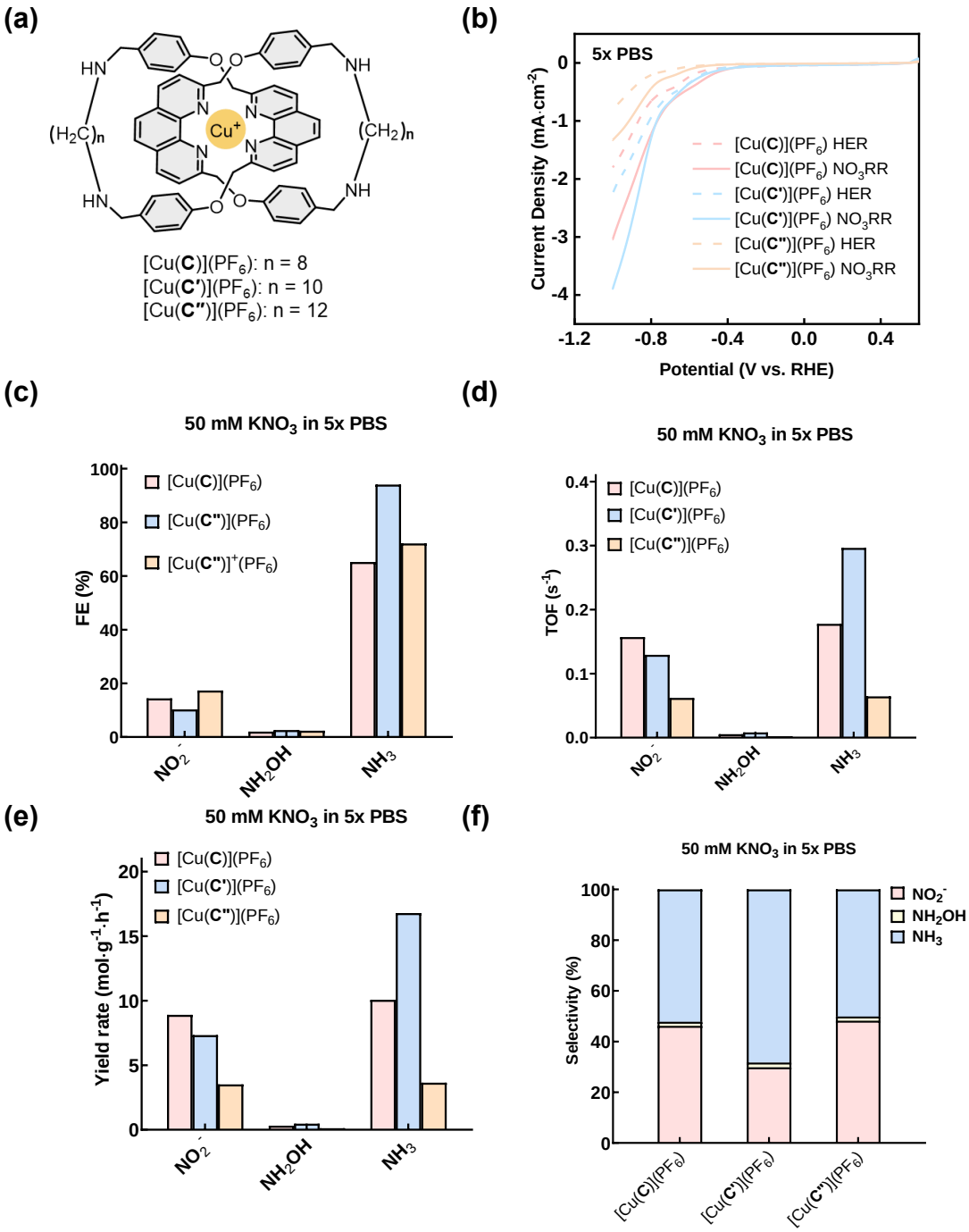

Figure 6. Impact of mechanical bond tightness on the electrocatalytic performance of Cu catenanes. (a) Structures of Cu(I) catenanes complexes with different sizes of the interlocked macrocycles. (b) Mass activity with NO_3RR (solid line) and HER (dashed line) in pH 7 Ar-saturated 5x PBS catalyzed by [Cu(**C**)](PF_6) (pink), [Cu(**C′**)](PF_6) (blue), and [Cu(**C″**)](PF_6) (orange). (c) Faradaic efficiency (FE), (d) turnover frequency (TOF), and (e) yield rates of NH_3, NH_2OH, and NO_2^- obtained by [Cu(**C**)](PF_6) (pink), [Cu(**C′**)](PF_6) (blue), and [Cu(**C″**)](PF_6) (orange) at -0.8 V vs. RHE. (f) Product selectivity of [Cu(**C**)](PF_6), [Cu(**C′**)](PF_6), and [Cu(**C″**)](PF_6) at -0.8 V vs. RHE.

Conclusions

A series of molecular Cu(I) complexes supported by catenane ligands tailored for efficient electrocatalytic NO_3RR have been developed. Cationic ammoniums were introduced to the catenane skeleton (i.e., [Cu(**C$_{6p}$**)]$(PF_6)_7$, [Cu(**C$_{4p}$**)]$(PF_6)_5$) to enhance the activity and selectivity of ammonia formation by facilitating nitrate binding and ammonia release. Electrochemical studies showed that [Cu(**C$_{6p}$**)]$(PF_6)_7$ supported by a hexacationic [2]catenane ligand selectively generated ammonia with a Faradaic efficiency reaching 86%, while the anionic control (i.e. [Cu(**C$_{4n}$**)](PF_6)) exhibited suppressed activity and selectivity. The ring size effect of the interlocked macrocycles was also investigated, and the medium-sized [Cu(**C′**)](PF_6) was found to exhibit better activity and selectivity than both the smaller [Cu(**C**)](PF_6) and the larger [Cu(**C″**)](PF_6). Taken together, these results suggest that catalyst performance can be enhanced via covalent modification (chemical) and mechanical interlocking (physical). Previous examples with Cu molecular complexes could only reduce nitrite but not nitrate, here for the first time, nitrate-to-ammonia conversion is realized by the ability of the Cu catenanes to overcome the initial nitrate-to-nitrite step. These results were valuable not only because of the rational design of Cu(I) complexes for efficient electrocatalytic reactions involving intricate proton-coupled electron transfer steps, but also the potential of mechanically interlocked ligands as a platform for transition metal catalyst customization with molecular features that are not easily achievable by non-interlocked analogues and conventional catalyst designs.

Experimental section

General Methods

Chemicals for synthesis were obtained from commercial sources and used as received unless otherwise stated. Sodium hydroxide (NaOH, analytical grade, Merck Millipore), Nafion perfluorinated resin solution (5 wt% in lower aliphatic alcohols and water, containing 15-20% water, Sigma-Aldrich), sodium nitrite ($NaNO_2$, Acros Organics), ammonium chloride (NH_4Cl, A.R. Dieckmann), phenol (C_6H_5OH, Sigma-Aldrich), sodium citrate anhydrous ($Na_3C_6H_5O_7$, J&K Scientific), sodium hypochlorite solution (NaClO solution, 11-14% available schlorine, Alfa Aesar), and sodium nitroprusside ($Na_2Fe(CN)_5NO{\cdot}2H_2O$, A.R. Beijing huagongchang). Electrochemical studies at pH 7 were performed in PBS buffer containing sodium chloride (NaCl, Dieckmann), potassium chloride

(KCl, J&K Scientific), sodium hydrogen phosphate (Na_2HPO_4, Dieckmann), and potassium dihydrogen phosphate (KH_2PO_4, Dieckmann). NO_3RR Experiments were conducted in the above PBS buffer with 50 mM potassium nitrate (KNO_3, Acros Organics). All buffer solutions were prepared using Milli-Q water (>18 MΩ cm) and were sparged with Ar (99.995% high purity grade, Linde HKO) for 30 min before each experiment following published methods.[28, 48, 53]

General inks preparation method

Vulcan XC-72 carbon black (Cabot) was pretreated and soaked in 0.1 M HCl (Duksan, 37% GR) for 24 h. The acid-treated carbon black was filtered and washed using Milli-Q ultrapure water, then dried in a vacuum oven at 80 °C overnight. [Cu(**C$_{4n}$**)](PF$_6$), [Cu(**C$_{4p}$**)](PF$_6$)$_5$, [Cu(**C$_{6p}$**)](PF$_6$)$_7$, [Cu(**C**)](PF$_6$), [Cu(**C′**)](PF$_6$) and [Cu(**C″**)](PF$_6$) were fully dissolved in acetonitrile (RCI Labscan, AR) and mixed with the pretreated Vulcan XC-72 to form their respective carbon mixtures (30% w/w). The mixtures were sonicated for 5 min. After sonication, the mixtures were dried under vacuum at 37 °C overnight. Finely ground [Cu(**C$_{4n}$**)](PF$_6$), [Cu(**C$_{4p}$**)](PF$_6$)$_5$, [Cu(**C$_{6p}$**)](PF$_6$)$_7$, [Cu(**C**)](PF$_6$), [Cu(**C′**)](PF$_6$) and [Cu(**C″**)](PF$_6$) catalysts on Vulcan XC-72 (4 mg) were suspended and sonicated in 1 mL ethanol (Scharlab, Abs) for 15 min, respectively. Nafion perfluorinated resin solution (4 µL, 5 wt% in lower aliphatic alcohols with 15−20% water, Sigma-Aldrich) was added into the well-dispersed catalyst/Vulcan in ethanol. The resulting mixture was then continuously sonicated for 10 min to form inks. 8 µL of the ink was drop-casted onto a glassy carbon electrode (A = 0.07065 cm^2, Gaoss Union) which was polished with 3 to 0.5 µm alumina suspension polishing kit (Allied Tech) and further dried under a stream of N_2.[48, 54-55]

Electrochemical Activity Measurements

Electrochemical studies were carried out using a CH Instruments 760E electrochemical workstation at room temperature following published procedures. Experiments were performed in a three-compartment cell with an aqueous Ag/AgCl (3 M KCl, CHI) reference electrode separated from the working electrode by a Luggin capillary as described previously.[56] Electrochemical potentials were reported relative to the reversible hydrogen electrode (RHE) using a published protocol. A Pt-wire counter electrode was separated from the working electrode by a glass frit. Chronoamperometric measurements were conducted at -0.8 V vs RHE in 5x PBS (685 mM NaCl,

13.5 mM KCl, 50 mM Na_2HPO_4 and 9 mM KH_2PO_4) buffer solution containing 50 mM KNO_3 for 0.5 h. The volume of the electrolyte in each chamber was 4 mL. Before electrochemical tests, the electrolyte solution was sparged with Ar for 30 min to remove dissolved O_2. Linear sweep voltammetry (LSV) was conducted at a scan rate of 10 mV s^{-1}. Electrolysis was performed at a given potential for a designated time period.[28]

Material Characterization

X-ray photoelectron spectroscopy (XPS) was conducted using a Thermo Scientific Escalab QXi +X-ray photoelectron spectrometer (XPS) microprobe, and the spectra were calibrated with a binding energy of 284.8 eV for C 1s. The data were analyzed following a published protocol.[54, 56] Ex-situ Cu L3-edge, X-ray absorption spectroscopy (XAS) measurements were conducted in total electron yield (TEY) mode at the TLS beamline 20A end station at the National Synchrotron Radiation Research Center (NSRRC).[57]

Product Analysis

Nitrate and nitrite concentrations were quantified using an ion chromatograph (IC) system (Thermo Scientific ICS-1100). NO_3^- and NO_2^- concentration was quantified by an ion chromatograph system (ICS-1100) with an electrochemical detector (ECD). 1000 ppm NO_3^- and NO_2^- stock solutions were prepared in Milli-Q ultrapure water and diluted to known concentration and injected into the IC system to obtain a series of peak areas. Standard curves were prepared by correlating the NO_3^- and NO_2^- concentration and the peak areas.[28]

All UV-Visible spectra were collected using an Implen Nanophotometer NP80 UV-Vis spectrophotometer with UVette (Eppendorf) cuvettes. Ammonia was quantified by an indophenol blue method.[58] Phenol (1.058 g) was dissolved in absolute ethanol (10 mL) to prepare fresh phenol solution, which can be used for a week. Sodium nitroprusside (0.05 g) was dissolved in Milli-Q water (10 mL) to prepare Fe catalyst solution. 5% NaClO solution was diluted from commercially available 11-14% NaClO using Milli-Q water. The alkaline citrate solution was prepared by dissolving NaOH (2.5 g) and trisodium citrate (50 g) in Milli-Q water (250 mL). The alkaline oxidizing solution was prepared by mixing the alkaline citrate solution and the 5% NaClO solution with a V/V ratio of 4:1. Ammonia standard solutions were prepared by diluting NH_4Cl stock solution (1000 ppm) into designated concentrations. Standard solution (0.5 mL) was diluted 5 folds using Milli-Q water. Phenol solution (0.1 mL), Fe catalyst

solution (0.1 mL), and alkaline oxidizing solution (0.425 mL) were sequentially added into the diluted standard solution. After mixing thoroughly, the final solution was placed in the dark at room temperature for 4 h. NH_4^+ standard curve was constructed by correlating standard solution concentrations with absorbances at 630 nm.[28, 59-60] The same procedure was used to quantify the amount of NH_4^+ in the electrolysis experiment.

Hydroxylamine was quantified by a revised method with $K_3Fe(CN)_6$ under strong alkaline condition. 0.2 mL sample or designed NH_2OH standard, 0.1 mL $K_3Fe(CN)_6$ in 100 mM KCl, and 0.3 mL 25% KOH were mixed thoroughly following the writing sequence and reacted for 7 min. A blank control was conducted by replacing sample with electrolyte only. NH_2OH standard curve was constructed by correlating standard solution concentrations with absorbances at 425 nm.[59]

Product Analysis Calculations

Faradaic Efficiency (%)

$$FE = \frac{n \times F \times C_{product} \times V}{Q} \times 100\% \qquad Eq\ 1$$

where $C_{product}$ is the concentration of each product in mol·L^{-1}, V is the volume of electrolyte solution (4 × 10^{-3} L), n is number of electrons of a certain product, F is Faraday constant (96485 C·mol^{-1}), and Q is the total charge (C) passed through the electrolysis reaction.

Turnover Frequency (s^{-1})

$$TOF = \frac{C_{product} \times V}{m_{catalyst} \times t} \qquad Eq\ 2$$

where $C_{product}$ is the concentration of each product in mol·L^{-1}, V is the volume of electrolyte solution (4 × 10^{-3} L), F is Faraday constant (96485 C·mol^{-1}), m is the number of moles in catalyst, and t is the electrolysis time in s.

Yield Rate (mol·g^{-1}·h^{-1})

$$Yield = \frac{C_{product} \times V}{M_{catalyst} \times t} \qquad Eq\ 3$$

where $C_{product}$ is the concentration of each product in mol·L^{-1}, V is the volume of electrolyte solution (4 x 10^{-3} L), $M_{catalyst}$ is the mass of Cu catalyst, and t is the electrolysis time in h.

Product Selectivity (%)

$$Selectivity = \left(\frac{moles\ of\ N_{product}}{Total\ moles\ of\ product}\right) \times 100\% \qquad Eq\ 4$$

$N_{product}$ refers to the nitrogenous product generated.

NO_3^- Conversion Rate (%)

$$\eta_{NO_3^-} = \frac{C_{0,NO_3^-} - C_{NO_3^-}}{C_{0,NO_3^-}} \times 100\% \qquad Eq\ 5$$

Methods for Kinetic Isotope Effect Studies

All proteo and deutero aqueous solutions were prepared freshly each day using Milli-Q water (>18 MΩ cm) and D_2O, respectively. For experiments in pH 7 and pD 7, both proteo and deutero PBS solutions containing sodium chloride (NaCl, Dieckmann), potassium chloride (KCl, J&K Scientific), sodium hydrogen phosphate (Na_2HPO_4, Dieckmann), and potassium dihydrogen phosphate (KH_2PO_4, Dieckmann) were used. NO_3RR experiments were conducted in the above PBS buffer with 50 mM potassium nitrate (KNO_3, Acros Organics). The pH and pD values of buffer solutions were measured using a Jenway 3510 Standard Digital pH Meter calibrated with three standard buffer solutions.[56, 61-63] pH readings were converted to pD using Eq 6:

$$pD = pH_a\ (apparent\ reading\ from\ pH\ meter) + 0.41 \qquad Eq\ 6$$

Associated content

Supporting Information

The Supporting Information is available free of charge.

The experimental data, as well as the characterization data for all of the compounds prepared in the course of these studies, experimental details, synthetic procedures, NMR and MS characterization data, control experiments, kinetic isotope effect studies, XPS, ICP-MS results, cyclic voltammograms, linear sweep voltammograms, computational methods and inresults, supplementary tables, additional notes, and supporting figures are available in the Supporting Information.

Author information

These authors contributed equally: Yulin Deng, Xiaoyong Mo.

Yulin Deng - Department of Chemistry, HKU-CAS Joint Laboratory of New Materials, University of Hong Kong, Hong Kong SAR, China; https://orcid.org/0000-0003-1566-3619
Xiaoyong Mo - Department of Chemistry, HKU-CAS Joint Laboratory of New Materials, University of Hong Kong, Hong Kong SAR, China; https://orcid.org/0000-0002-8586-4056
Samuel Kin-Man Lai - Department of Chemistry, HKU-CAS Joint Laboratory of New Materials, University of Hong Kong, Hong Kong SAR, China; https://orcid.org/0000-0002-8959-724X
Shu-Chih Haw - National Synchrotron Radiation Research Center, 101 Hsin-Ann Road, Hsinchu 30076, Taiwan

Corresponding authors
Edmund C. M. Tse - Department of Chemistry, HKU-CAS Joint Laboratory of New Materials, University of Hong Kong, Hong Kong SAR, China; https://orcid.org/0000-0002-9313-1290; Email: ecmtse@hku.hk
Ho Yu Au-Yeung - Department of Chemistry, HKU-CAS Joint Laboratory of New Materials, University of Hong Kong, Hong Kong SAR, China; State Key Laboratory of Synthetic Chemistry, University of Hong Kong, Hong Kong, China; https://orcid.org/0000-0002-7216-7921; Email: hoyuay@hku.hk

Author Contributions
Y.D. and X.M. performed the conceptualization, methodology, experimental investigation, formal analysis, writing, reviewing and editing of the manuscript; S.K.-M.L. performed computational investigations. S.-C.H. assisted in the XAS experiments; H.Y.A.-Y. and E.C.M.T. supervised and administrated the project, performed the conceptualization, methodology, formal analysis, data visualization, acquired funding, wrote, reviewed and edited the manuscript.

Notes
The authors declare no competing financial interest.

Acknowledgments
E.C.M.T. would like to express gratitude to the Innovation Technology Commission for an ITSP Seed Project (ITC: ITS/271/22) on an interfacial electrocatalysis project. H.Y.A.-Y. acknowledges the supports from the CAS-Croucher Funding Scheme for Joint Laboratories and the Collaborative

Research Fund (C7075-21G) from the Research Grants Councils (RGC) of Hong Kong. X.M. thanks the support from the Shenzhen Science and Technology Innovation Commission (SZSTI: JCYJ20210324122011031). Y.D. acknowledges the Dissertation Year Fellowship from The University of Hong Kong. The authors thank Frankie Y.F. Chan at the Electron Microscope Unit (EMU) at the University of Hong Kong (HKU) for his help with materials characterization supported by Innovation Technology Fund (ITF: TSSSU/HKU/23/05/2). X.M. and E.C.M.T. acknowledge the funding support from "Laboratory for Synthetic Chemistry and Chemical Biology" under the Health@InnoHK Program launched by ITC, HKSAR, China. The authors also thank the RGC in Hong Kong for a Theme-based Research Scheme (TRS: T23-713/22-R), an Early Career Scheme (ECS: 27301120), and a General Research Fund (GRF: 17308323) for enhancing the surface characterization facility at the HKU-CAS Joint Laboratory on New Materials and supporting research activities on green electrocatalysis and clean energy conversion. UGC funding administered by The University of Hong Kong is acknowledged for support of the Electrospray Ionisation Quadrupole Time-of-Flight Mass Spectrometry Facilities under the support for Interdisciplinary Research in Chemical Science. S.K.-M.L. thanks the High-Performance Computing (HPC) services offered by ITS at HKU.

REFERENCES

(1) Rosca, V.; Duca, M.; de Groot, M. T.; Koper, M. T. M., Nitrogen Cycle Electrocatalysis. *Chem. Rev.* **2009,** *109*, 2209-2244.

(2) Chen, F.-Y.; Elgazzar, A.; Pecaut, S.; Qiu, C.; Feng, Y.; Ashokkumar, S.; Yu, Z.; Sellers, C.; Hao, S.; Zhu, P.; Wang, H., Electrochemical nitrate reduction to ammonia with cation shuttling in a solid electrolyte reactor. *Nat. Catal.* **2024**.

(3) Liu, Y.; Liu, K.; Wang, P.; Jin, Z.; Li, P., Electrocatalytic upcycling of nitrogenous wastes into green ammonia: advances and perspectives on materials innovation. *Carbon Neutrality* **2023,** *2*, 14.

(4) Belhamidi, S.; El-Ghzizel, S.; Taky, M.; Elmidaoui, A., Nitrate removal of groundwater by reverse osmosis, nanofiltration and electrodialysis: performances and cost comparison. *Desalin. Water Treat.* **2022,** *262*, 338-346.

(5) Pang, Y.; Wang, J., Various electron donors for biological nitrate removal: A review. *Sci. Total Environ.* **2021,** *794*, 148699.

(6) Scholes, R. C.; Vega, M. A.; Sharp, J. O.; Sedlak, D. L., Nitrate removal from reverse osmosis concentrate in pilot-scale open-water unit process wetlands. *Environ. Sci.: Water Res. Technol.* **2021,** *7*, 650-661.

(7) Aliaskari, M.; Schäfer, A. I., Nitrate, arsenic and fluoride removal by electrodialysis from brackish groundwater. *Water Res.* **2021,** *190*, 116683.
(8) Chen, J.; Gu, M.; Zhou, Y.; Wan, D.; He, Q.; Shi, Y.; Liu, Y., Efficient nitrate and perchlorateremoval from aqueous solution via a novel electro-dialysis ion-exchange membrane bioreactor. *J. Chem. Eng.* **2022,** *430*, 132952.
(9) Ahmed, S. M.; Rind, S.; Rani, K., Systematic review: External carbon source for biological denitrification for wastewater. *Biotechnol Bioeng.* **2023,** *120*, 642-658.
(10) Fan, Y.; Wang, X.; Butler, C.; Kankam, A.; Belgada, A.; Simon, J.; Gao, Y.; Chen, E.; Winter, L. R., Highly efficient metal-free nitrate reduction enabled by electrified membrane filtration. *Nat. Water* **2024,** *2*, 684-696.
(11) Bai, L.; Franco, F.; Timoshenko, J.; Rettenmaier, C.; Scholten, F.; Jeon, H. S.; Yoon, A.; Rüscher, M.; Herzog, A.; Haase, F. T.; Kühl, S.; Chee, S. W.; Bergmann, A.; Beatriz, R. C., Electrocatalytic Nitrate and Nitrite Reduction toward Ammonia Using Cu_2O Nanocubes: Active Species and Reaction Mechanisms. *J. Am. Chem. Soc.* **2024,** *146*, 9665-9678.
(12) Chen, D.; Yin, D.; Zhang, S.; Yip, S.; Ho, J. C., Nitrate electroreduction: recent development in mechanistic understanding and electrocatalyst design. *Mater. Today Energy* **2024,** *44*, 101610.
(13) Gao, X.; Tse, E. C. M., Unraveling the Performance Descriptors for Designing Single-Atom Catalysts on Defective MXenes for Exclusive Nitrate-To-Ammonia Electrocatalytic Upcycling. *Small* **2024,** *20*, 2306311.
(14) Ricke, N. D.; Murray, A. T.; Shepherd, J. J.; Welborn, M. G.; Fukushima, T.; Van Voorhis, T.; Surendranath, Y., Molecular-Level Insights into Oxygen Reduction Catalysis by Graphite-Conjugated Active Sites. *ACS Catal.* **2017,** *7*, 7680-7687.
(15) Elwell, C. E.; Gagnon, N. L.; Neisen, B. D.; Dhar, D.; Spaeth, A. D.; Yee, G. M.; Tolman, W. B., Copper–Oxygen Complexes Revisited: Structures, Spectroscopy, and Reactivity. *Chem. Rev.* **2017,** *117*, 2059-2107.
(16) Zhang, S.; Wu, J.; Zheng, M.; Jin, X.; Shen, Z.; Li, Z.; Wang, Y.; Wang, Q.; Wang, X.; Wei, H.; Zhang, J.; Wang, P.; Zhang, S.; Yu, L.; Dong, L.; Zhu, Q.; Zhang, H.; Lu, J., Fe/Cu diatomic catalysts for electrochemical nitrate reduction to ammonia. *Nat. Commun.* **2023,** *14*, 3634.
(17) Daiyan, R.; Tran-Phu, T.; Kumar, P.; Iputera, K.; Tong, Z.; Leverett, J.; Khan, M. H. A.; Asghar Esmailpour, A.; Jalili, A.; Lim, M.; Tricoli, A.; Liu, R.-S.; Lu, X.; Lovell, E.; Amal, R., Nitrate reduction to ammonium: from CuO defect engineering to waste NOx-to-NH_3 economic feasibility. *Energy Environ. Sci.* **2021,** *14*, 3588-3598.

(18) Jia, R.; Wang, Y.; Wang, C.; Ling, Y.; Yu, Y.; Zhang, B., Boosting Selective Nitrate Electroreduction to Ammonium by Constructing Oxygen Vacancies in TiO_2. *ACS Catal.* **2020,** *10*, 3533-3540.
(19) Garcia-Segura, S.; Lanzarini-Lopes, M.; Hristovski, K.; Westerhoff, P., Electrocatalytic reduction of nitrate: Fundamentals to full-scale water treatment applications. *Appl. Catal. B* **2018,** *236*, 546-568.
(20) Fang, Z.; Jin, Z.; Tang, S.; Li, P.; Wu, P.; Yu, G., Porous Two-dimensional Iron-Cyano Nanosheets for High-rate Electrochemical Nitrate Reduction. *ACS Nano* **2022,** *16*, 1072-1081.
(21) Martínez, J.; Ortiz, A.; Ortiz, I., State-of-the-art and perspectives of the catalytic and electrocatalytic reduction of aqueous nitrates. *Appl. Catal. B* **2017,** *207*, 42-59.
(22) Han, S.; Li, H.; Li, T.; Chen, F.; Yang, R.; Yu, Y.; Zhang, B., Ultralow overpotential nitrate reduction to ammonia via a three-step relay mechanism. *Nat. Catal.* **2023,** *6*, 402-414.
(23) de Groot, M. T.; Koper, M. T. M., The influence of nitrate concentration and acidity on the electrocatalytic reduction of nitrate on platinum. *J. Electroanal. Chem.* **2004,** *562*, 81-94.
(24) Yang, J.; Sebastian, P.; Duca, M.; Hoogenboom, T.; Koper, M. T. M., pH dependence of the electroreduction of nitrate on Rh and Pt polycrystalline electrodes. *Chem. Commun.* **2014,** *50*, 2148-2151.
(25) Bullock, R. M.; Chen, J. G.; Gagliardi, L.; Chirik, P. J.; Farha, O. K.; Hendon, C. H.; Jones, C. W.; Keith, J. A.; Klosin, J.; Minteer, S. D., Using nature's blueprint to expand catalysis with Earth-abundant metals. *Science* **2020,** *369*, eabc3183.
(26) Gao, Q.; Pillai, H. S.; Huang, Y.; Liu, S.; Mu, Q.; Han, X.; Yan, Z.; Zhou, H.; He, Q.; Xin, H.; Zhu, H., Breaking adsorption-energy scaling limitations of electrocatalytic nitrate reduction on intermetallic CuPd nanocubes by machine-learned insights. *Nat. Commun.* **2022,** *13*, 2338.
(27) Chipoco Haro, D. A.; Barrera, L.; Iriawan, H.; Herzog, A.; Tian, N.; Medford, A. J.; Shao-Horn, Y.; Alamgir, F. M.; Hatzell, M. C., Electrocatalysts for Inorganic and Organic Waste Nitrogen Conversion. *ACS Catal.* **2024,** *14*, 9752-9775.
(28) Wang, W.; Chen, J.; Tse, E. C. M., Synergy between Cu and Co in a Layered Double Hydroxide Enables Close to 100% Nitrate-to-Ammonia Selectivity. *J. Am. Chem. Soc.* **2023,** *145*, 26678-26687.
(29) Wang, K.; Mao, R.; Liu, R.; Zhang, J.; Zhao, H.; Ran, W.; Zhao, X., Intentional corrosion-induced reconstruction of defective NiFe layered double

hydroxide boosts electrocatalytic nitrate reduction to ammonia. *Nat. Water* **2023,** *1*, 1068-1078.
(30) van Langevelde, P. H.; Engbers, S.; Buda, F.; Hetterscheid, D. G. H., Elucidation of the Electrocatalytic Nitrite Reduction Mechanism by Bio-Inspired Copper Complexes. *ACS Catal.* **2023,** *13*, 10094-10103.
(31) Valdez, C. E.; Smith, Q. A.; Nechay, M. R.; Alexandrova, A. N., Mysteries of Metals in Metalloenzymes. *Acc. Chem. Res.* **2014,** *47*, 3110-3117.
(32) Suzuki, S.; Kataoka, K.; Yamaguchi, K.; Inoue, T.; Kai, Y., Structure–function relationships of copper-containing nitrite reductases. *Coord. Chem. Rev.* **1999,** *190-192*, 245-265.
(33) Van Stappen, C.; Deng, Y.; Liu, Y.; Heidari, H.; Wang, J.-X.; Zhou, Y.; Ledray, A. P.; Lu, Y., Designing Artificial Metalloenzymes by Tuning of the Environment beyond the Primary Coordination Sphere. *Chem. Rev.* **2022,** *122*, 11974-12045.
(34) Yu, Y.; Lv, X.; Li, J.; Zhou, Q.; Cui, C.; Hosseinzadeh, P.; Mukherjee, A.; Nilges, M. J.; Wang, J.; Lu, Y., Defining the Role of Tyrosine and Rational Tuning of Oxidase Activity by Genetic Incorporation of Unnatural Tyrosine Analogs. *J. Am. Chem. Soc.* **2015,** *137*, 4594-4597.
(35) Trammell, R.; Rajabimoghadam, K.; Garcia-Bosch, I., Copper-Promoted Functionalization of Organic Molecules: from Biologically Relevant Cu/O_2 Model Systems to Organometallic Transformations. *Chem. Rev.* **2019,** *119*, 2954-3031.
(36) Santini, C.; Pellei, M.; Gandin, V.; Porchia, M.; Tisato, F.; Marzano, C., Advances in Copper Complexes as Anticancer Agents. *Chem. Rev.* **2014,** *114*, 815-862.
(37) Albrecht-Gary, A. M.; Saad, Z.; Dietrich-Buchecker, C. O.; Sauvage, J. P., Interlocked macrocyclic ligands: a kinetic catenand effect in copper(I) complexes. *J. Am. Chem. Soc.* **1985,** *107*, 3205-3209.
(38) Dietrich-Buchecker, C. O.; Kern, J.-M.; Sauvage, J.-P., An air-stable d9 nickel(I) catenate: stabilisation of monovalent nickel by interlocked macrocyclic ligands. *J. Chem. Soc., Chem. Commun.* **1985**, 760-762.
(39) Dietrich-Buchecker, C.; Sauvage, J. P.; Kern, J. M., Synthesis and electrochemical studies of catenates: stabilization of low oxidation states by interlocked macrocyclic ligands. *J. Am. Chem. Soc.* **1989,** *111*, 7791-7800.
(40) Cirulli, M.; Kaur, A.; Lewis, J. E. M.; Zhang, Z.; Kitchen, J. A.; Goldup, S. M.; Roessler, M. M., Rotaxane-Based Transition Metal Complexes: Effect of the Mechanical Bond on Structure and Electronic Properties. *J. Am. Chem. Soc.* **2019,** *141*, 879-889.

(41) Albrecht-Gary, A. M.; Dietrich-Buchecker, C.; Saad, Z.; Sauvage, J. P., Topological kinetic effects: complexation of interlocked macrocyclic ligands by cationic species. *J. Am. Chem. Soc.* **1988,** *110*, 1467-1472.
(42) Sauvage, J. P., Interlacing molecular threads on transition metals: catenands, catenates, and knots. *Acc. Chem. Res.* **1990,** *23*, 319-327.
(43) Lewis, J. E. M.; Beer, P. D.; Loeb, S. J.; Goldup, S. M., Metal ions in the synthesis of interlocked molecules and materials. *Chem. Soc. Rev.* **2017,** *46*, 2577-2591.
(44) Beves, J. E.; Blight, B. A.; Campbell, C. J.; Leigh, D. A.; McBurney, R. T., Strategies and Tactics for the Metal-Directed Synthesis of Rotaxanes, Knots, Catenanes, and Higher Order Links. *Angew. Chem. Int. Ed.* **2011,** *50*, 9260-9327.
(45) Gao, W.-X.; Feng, H.-J.; Guo, B.-B.; Lu, Y.; Jin, G.-X., Coordination-Directed Construction of Molecular Links. *Chem. Rev.* **2020,** *120*, 6288-6325.
(46) Au-Yeung, H. Y.; Deng, Y., Distinctive features and challenges in catenane chemistry. *Chem. Sci.* **2022,** *13*, 3315-3334.
(47) Zhu, L.; Li, J.; Yang, J.; Au-Yeung, H. Y., Cross dehydrogenative C–O coupling catalysed by a catenane-coordinated copper(I). *Chem. Sci.* **2020,** *11*, 13008-13014.
(48) Mo, X.; Deng, Y.; Lai, S. K.-M.; Gao, X.; Yu, H.-L.; Low, K.-H.; Guo, Z.; Wu, H.-L.; Au-Yeung, H. Y.; Tse, E. C. M., Mechanical Interlocking Enhances the Electrocatalytic Oxygen Reduction Activity and Selectivity of Molecular Copper Complexes. *J. Am. Chem. Soc.* **2023,** *145*, 6087-6099.
(49) Hsueh, F.-C.; Tsai, C.-Y.; Lai, C.-C.; Liu, Y.-H.; Peng, S.-M.; Chiu, S.-H., N-Heterocyclic Carbene Copper(I) Rotaxanes Mediate Sequential Click Ligations with All Reagents Premixed. *Angew. Chem. Int. Ed.* **2020,** *59*, 11278-11282.
(50) Fan, J.; Arrazolo, L. K.; Du, J.; Xu, H.; Fang, S.; Liu, Y.; Wu, Z.; Kim, J.-H.; Wu, X., Effects of Ionic Interferents on Electrocatalytic Nitrate Reduction: Mechanistic Insight. *Environ. Sci. Tech.* **2024,** *58*, 12823-12845.
(51) Tang, M. P.; Zhu, L.; Deng, Y.; Shi, Y.-X.; Kin-Man Lai, S.; Mo, X.; Pang, X.-Y.; Liu, C.; Jiang, W.; Tse, E. C. M.; Au-Yeung, H. Y., Water and Air Stable Copper(I) Complexes of Tetracationic Catenane Ligands for Oxidative C−C Cross-Coupling. *Angew. Chem. Int. Ed.* **2024,** *63*, e202405971.
(52) Yee, C.-C.; Ng, A. W. H.; Au-Yeung, H. Y., Control over the macrocyclisation pathway and product topology in a copper-templated catenane synthesis. *Chem. Commun.* **2019,** *55*, 6169-6172.
(53) Wang, S.; Gao, X.; Mo, X.; Phillips, D. L.; Tse, E. C. M., Immobilization

of a Molecular Copper Complex and a Carboxylate-Terminated Cocatalyst on a Metal Oxide Electrode for Enhanced Electrocatalytic Oxygen Reduction. *ACS Catal.* **2023,** *13*, 5599-5608.

(54) Varnell, J. A.; Tse, E. C. M.; Schulz, C. E.; Fister, T. T.; Haasch, R. T.; Timoshenko, J.; Frenkel, A. I.; Gewirth, A. A., Identification of carbon-encapsulated iron nanoparticles as active species in non-precious metal oxygen reduction catalysts. *Nat. Commun.* **2016,** *7*, 12582.

(55) Tse, E. C. M.; Schilter, D.; Gray, D. L.; Rauchfuss, T. B.; Gewirth, A. A., Multicopper Models for the Laccase Active Site: Effect of Nuclearity on Electrocatalytic Oxygen Reduction. *Inorg. Chem.* **2014,** *53*, 8505-8516.

(56) Mo, X.; Gao, X.; Gillado, A. V.; Chen, H.-Y.; Chen, Y.; Guo, Z.; Wu, H.-L.; Tse, E. C. M., Direct 3D Printing of Binder-Free Bimetallic Nanomaterials as Integrated Electrodes for Glycerol Oxidation with High Selectivity for Valuable C3 Products. *ACS Nano* **2022,** *16*, 12202-12213.

(57) Chou, T.-C.; Chang, C.-C.; Yu, H.-L.; Yu, W.-Y.; Dong, C.-L.; Velasco-Vélez, J.-J.; Chuang, C.-H.; Chen, L.-C.; Lee, J.-F.; Chen, J.-M.; Wu, H.-L., Controlling the Oxidation State of the Cu Electrode and Reaction Intermediates for Electrochemical CO_2 Reduction to Ethylene. *J. Am. Chem. Soc.* **2020,** *142*, 2857-2867.

(58) Wang, Y.; Xu, A.; Wang, Z.; Huang, L.; Li, J.; Li, F.; Wicks, J.; Luo, M.; Nam, D.-H.; Tan, C.-S.; Ding, Y.; Wu, J.; Lum, Y.; Dinh, C.-T.; Sinton, D.; Zheng, G.; Sargent, E. H., Enhanced Nitrate-to-Ammonia Activity on Copper–Nickel Alloys via Tuning of Intermediate Adsorption. *J. Am. Chem. Soc.* **2020,** *142*, 5702-5708.

(59) Wang, W.; Tse, E. C. M., Enhanced Nitrite Electrovalorization to Ammonia by a NiFe Layered Double Hydroxide. *Eur. J. Inorg. Chem.* **2022,** *2022*, e202200291.

(60) Jiang, Z.; Wang, Y.; Lin, Z.; Yuan, Y.; Zhang, X.; Tang, Y.; Wang, H.; Li, H.; Jin, C.; Liang, Y., Molecular electrocatalysts for rapid and selective reduction of nitrogenous waste to ammonia. *Energy Environ. Sci.* **2023,** *16*, 2239-2246.

(61) Guo, D.-S.; Uzunova, V. D.; Su, X.; Liu, Y.; Nau, W. M., Operational calixarene-based fluorescent sensing systems for choline and acetylcholine and their application to enzymatic reactions. *Chem. Sci.* **2011,** *2*, 1722-1734.

(62) Barile, C. J.; Tse, E. C. M.; Li, Y.; Sobyra, T. B.; Zimmerman, S. C.; Hosseini, A.; Gewirth, A. A., Proton switch for modulating oxygen reduction by a copper electrocatalyst embedded in a hybrid bilayer membrane. *Nat. Mater.* **2014,** *13*, 619-623.

(63) Tse, E. C. M.; Hoang, T. T. H.; Varnell, J. A.; Gewirth, A. A., Observation

of an Inverse Kinetic Isotope Effect in Oxygen Evolution Electrochemistry. *ACS Catal.* **2016,** *6*, 5706-5714.

Graphical abstract

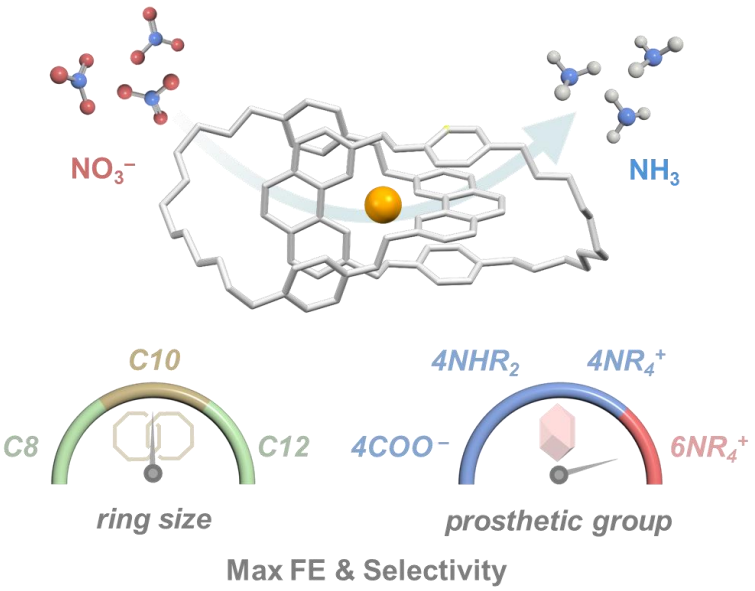

Synopsis

Molecular Cu(I) complexes supported by [2]catenane ligands with well-defined coordination structures are mechanically and covalently tailored as electrocatalysts for nitrate reduction. Introducing cationic ammoniums to the catenane skeleton enhances the activity and selectivity of ammonia formation by facilitating nitrate binding and ammonia release.